Scientific paper

Computational Molecular Modeling Studies of Some *Mycobacterium Tuberculosis* Alanine Racemase Inhibitors

Unni Jayaram* and Mohammed Afzal Azam

Department of Pharmaceutical Chemistry, JSS College of Pharmacy, Udhagamandalam - 643001, Tamil Nadu, India (A Constituent College of JSS Academy of Higher Education and Research, Mysuru).

* Corresponding author: E-mail: jayaramkvt@gmail.com

Received: 11-10-2021

Running title: Mycobacterium tuberculosis alanine racemase.

Abstract

Alanine racemase is a pyridoxal-5´-phosphate dependent bacterial enzyme that provides the essential peptidoglycan precursor D-alanine, utilized for cell wall synthesis. This enzyme is ubiquitous throughout bacteria, including *Mycobacterium tuberculosis*, making it an attractive target for antibacterial drug discovery. We investigated the binding mode of twenty five reported *Mycobacterium tuberculosis* alanine racemase inhibitors. The results obtained from molecular docking studies emphasized the importance of inhibitor interaction with Lys42, Tyr46, Arg140, His172 and Tyr175 residues at the catalytic binding pocket of alanine racemase enzyme. The predicted binding free energies showed that van der Waals and nonpolar solvation interactions are the driving force for binding of inhibitors. Molecular dynamics simulation studies of four such inhibitor-alanine racemase systems were further explored to study the inhibition mechanism. The quantum chemical parameters calculated at the B3LYP/6-31G**++ level of theory indicated that the inhibitors must have low values of the lowest unoccupied molecular orbital energy and high values of electrostatic potential for stronger interactions. We expect that this study can provide significant theoretical guidance for design of potent *Mycobacterium tuberculosis* alanine racemase inhibitors in future.

Keywords: Molecular docking; binding free energy; alanine racemase; molecular dynamics simulations.

1. Introduction

One-third of world's population is infected with Mycobacterium tuberculosis (M. tuberculosis) and remains a serious global health concern. Hence, discovery and development of effective chemotherapeutic agents against M. tuberculosis is of top health priority. Alanine racemase (AlaR) is a pyridoxal-5'-phosphate (PLP) dependent enzyme required for bacterial cell wall synthesis. This enzyme catalyses the conversion of L-alanine to D-alanine which is required for the synthesis of the peptidoglycan in both Gram-positive and Gram-negative bacteria.² Generally, AlaR is absent in higher eukaryotes but is ubiquitous throughout bacteria. Its inhibition is lethal to prokaryotes, hence making it an attractive target for the antibacterial drug discovery.3 This enzyme exists as a homodimer in which two monomers interact in a head-totail fashion, making two active sites, where PLP and alanine bind. AlaR from numerous bacteria has been structurally characterized including M. tuberculosis ala-

nine racemase (MtAlaR).4 The substrate entryway and active site of enzymes are shown to be highly conserved.^{5,6} The 3D crystal structure of MtAlaR monomer consists of 384 residues and two different domains. ⁴ The *N*-terminal domain is made up of an eight-stranded α/β -barrel from residues 1–246 and the C-terminal domain contains predominantly β -strands formed by residues 247–384. The approximate 130° angle between the N- and C- terminal domains is unique for MtAlaR. The substrate binding cavity having cofactor PLP390 forms an internal aldimine linkage with the highly conserved catalytic Lys42 residue which is surrounded by the side chains of Tyr175, Tyr46 and Tyr364. The binding cavity of this enzyme is compact $(5.5 \text{ Å} \times 5.0 \text{ Å} \times 2.5 \text{ Å})$, making it difficult for the larger molecules to reach the active site. The putative substrate binding site of MtAlaR exhibits structural similarity with AlaR binding sites of Pseudomonas aeruginosa, 4 Geobacillus stearothermophilus⁷ and Staphylococcus aureus.^{8,9} MtAlaR uses Lys42 and Tyr271 for the racemization reaction. 10-12 Site-directed mutagenesis and kinetic studies

revealed that Tyr271 serves as the base acting on the L-enantiomer¹³ and Lys42 on the antipode. It also showed that mutation of Arg219 to a glutamate residue reduced the pH independent Kcat value by more than 3 orders of magnitude¹¹ which is supported qualitatively by the quantum chemical calculations.¹² Several reports described the role of key binding residues Lys42, Tyr46, His172, Arg228, Tyr271 and Met319 in the enzyme catalytic steps.^{5,7,13,14} The amino acid residues outside the binding site but near to the entryway of the active site are highly conserved⁴ and can be exploited for the design of larger and potentially more specific inhibitors.

There are several well-known inhibitors of AlaR. Among them D-cycloserine and O-carbamyl-D-serine are two natural compounds known to inhibit AlaR. 15,16 But only D-cycloserine is approved commercially for the treatment of tuberculosis. However, its clinical use is limited due to severe toxic effects arising due to the lack of target specificity.¹⁷ D-cycloserine inhibits alanine racemase by interacting with the enzyme-bound co-factor PLP. There are several PLP dependent enzymes in nature, hence D-cycloserine is not target-specific. Several structural modifications of D,L-cycloserine have been made to improve the activity and target specificity but not to date resulted in development of AlaR specific inhibitors 18a,b with high potency. Several other scaffolds have also been investigated as AlaR inhibitors. These include β,β,β -trifluoroalanine, alanine phosphonate, 19 1-amino-cyclopropane phosphonate, 20 β -chloro- and β -fluoroalanine, 21 phosphonopeptides,^{22,23} and thiadiazolidinones.²⁴ Most of the substrate analogs, like D-cycloserine engage co-factor PLP.

The interest in identifying small molecule inhibitors of AlaR to overcome the liabilities of the existing compounds has intensified the structure-based drug design approach.^{25,26} In addition, there is a considerable research effort to discover AlaR inhibitors that are not substrate analogs and that act through different mechanisms of enzyme inhibition.^{24,27} In this study, we present the results of molecular docking, binding free-energy calculation, molecular dynamics (MD) simulation and quantum chemical calculation on literature reported MtAlaR inhibitors to get further insight into the binding mechanism of these inhibitors. The role of hydrogen bonding with key residues of MtAlaR catalytic pocket with these inhibitors is examined in detail. Binding free energies of protein with inhibitors were calculated by molecular mechanics-generalized born/surface area (MM-GBSA) and analysed. MD simulations were performed to investigate the stability and dynamical changes of predicted binding conformations. Using B3LYP/6-31G**++ level of theory, quantum chemical parameters were calculated to understand the mechanism of interaction between inhibitors and biological system. The information from this study provides further insight into the key structural features required to design or optimize alanine racemase inhibitors.

2. Materials and Methods

Computational Methods

2. 1. Molecular Docking

Twenty-five MtAlaR inhibitors (1-25) with wide range biological activity and structural diversity (Supplementary Table S1) were collected from literatures^{24,27} (Table 1) and used in the present study. The 3D structures of ligands were generated using the builder panel in Maestro 10.5 and subsequently optimized with the LigPrep module (Schrödinger 2017-2, LLC, New York, NY). Partial atomic charges were ascribed and possible ionization states were generated at a pH of 7.0. The energy minimization for each ligand was performed using OPLS3 force field.²⁸ The structure of MtAlaR (PDB-ID: 1XFC, 1.9 Å resolution) was retrieved from the protein data bank and prepared using protein preparation wizard²⁹ (Epik v4.0, Schrödinger 2017-2). Crystallographic water molecules (less than 3 hydrogen bonds) were deleted and hydrogen bonds (corresponding to pH 7.0) were added. Missing side chain atoms were added and breaks present in the structure were built using Prime (v4.8, Schrödinger 2017-2).³⁰ Then the energy of protein was minimized under OPLS3 force field²⁸ with the convergence of heavy atoms to a RMSD of 0.3 Å. The Ramachandran plot³¹ (Supplementary figure S1) showed 97.90% of the residues in the most favoured regions and none of the non-glycine residues in disallowed regions. The active site was defined with a 10 Å radius around the Lys42 residue present in the crystal structure and a grid box was generated at the centroid of this active site for docking. All compounds were docked into the catalytic pocket of prepared protein using Glide (v7.5, Schrödinger 2017-2)³² in extra precision (XP) mode without applying any constraints (Figure 1a-d and Supplementary figure S2). Best docked structures were selected based on Glide score function, Glide energy and Glide model energy (Supplementary Table S2). The best pose of 10, 19, 21 and 25/1XFC complexes were selected to run the molecular dynamics. Further, electrostatic potential surfaces for 21 and 25 (Supplementary figure S3a and S3b) and hydrophobic and hydrophilic map for 19, 21 and 25 (Supplementary figure S3c) were generated in the binding pocket of 1XFC enzyme.

2. 2. Binding Free Energy Calculation

Molecular mechanics-generalized born surface area (MM-GBSA) method is used to calculate the binding free energies of macromolecules, and serve as a powerful tool for the design of inhibitors.³³ The XP-molecular docking receptor-ligand complex structures ranking were minimized with Prime (v4.8, Schrödinger 2017-2).³⁰ Binding free energies of complexes were computed using MM-GB-SA continuum solvent model (Table 1) with OPLS3 force field²⁸ and VSGB 2.0 solvation model.³⁴

2. 3. Quantum Chemical Parameters

The molecular electrostatic potential (MEP)³⁵ calculations provide detailed stereoelectronic information and are useful to study the biological activity of a compound.³⁶ We calculated mean MEP of best binding conformations of inhibitors 1-25 by Jaguar (v9.1, Schrödinger 2017-2) using basis set 6-31G**++ and hybrid density functional theory with Hamiltonian-Nonrelativistic correlation functional (B3LYP) in gas phase. ESP maps of compounds 19, 21 and 25, which is an estimate of overall molecular size and location of regions of negative and positive electrostatic potential are shown in supplementary figure 4a-c. The deepest red color represents the most electronegative potential, whereas deepest blue indicates the most positive potential site in inhibitors.³⁷ A semi-empirical Neglect of Diatomic Differential Overlap (NDDO) module with RM138 method and RHF wave function (Schrödinger 2017-2) was used to calculate highest occupied molecular orbital (HOMO), lowest unoccupied molecular orbital (LUMO), electrophilic, nucleophilic and radical super delocalizibility energies (Supplementary Table S3). The frontier molecule orbital density distributions of HOMO and LUMO for compounds 19, 21 and 25 are shown in supplementary figure S5.

2. 4. Molecular Dynamics Simulations

In order to investigate the stability of the XP-docked inhibitor 10, 19, 21 and 25/1XFC complexes, 10 ns molecular dynamics simulations³⁹ were performed using the Desmond (v5.0) computational package. The systems were explicitly solvated in orthorhombic boxes (volume $10/1XFC = 460130 \text{ Å}^3$; volume $19/1XFC = 1016870 \text{ Å}^3$; volume $21/1XFC = 459351 \text{ Å}^3$; $25/1XFC = 985370 \text{ Å}^3$) with a shell of TIP4P40a,b water molecules within Desmond molecular dynamics system and allowing for a 10 Å buffer region between protein atoms and box sides. Overlapping water molecules were deleted and the systems were neutralized by counter ions. The total numbers of atoms in solvated protein structures of 10, 19, 21 and 25/1XFC complexes for the MD simulations are 43992, 44104, 44348 and 42692, respectively. Each system was placed at a distance of 10 Å from the edge of the box and LBFGS minimization was performed with 3 vectors and minimum 10 steepest descent steps until a gradient threshold of 25 kcal/ mol/Å was reached. Smooth particle mesh Ewald⁴¹ method was used for long range electrostatic interactions at a tolerance of 1e-09 and a cut-off radius of 9 Å was selected for short range electrostatic interactions. After minimization, systems were gradually heated in the NPT ensemble to 300° K with a time step of 2 fs. For bonded, near nonbonded, and far nonbonded interactions, a multiple time step RESPA integration algorithm was used throughout the dynamics with time steps of 2, 2 and 6 fs, respectively. Systems were then subjected to 10 ns MD simulations in the NPT ensemble (T = 300° K, thermostat relaxation time

= 200 ps; P = 1 atm; barostat relaxation time = 200 ps) using a Nose-Hoover thermostat⁴² and Martyna-Tobias-Klein barostat.⁴³ For each system, trajectories and 3D structures were visually analysed using the Maestro graphical interface.

3. Results and Discussion

3. 1. Molecular Docking

We compared different XP-docked poses (Figure 1 and also Supplementary figure S2) for the better understanding of interactions between MtAlaR and its inhibitors 1-25. It is evident that most of these inhibitors adopt similar hydrogen bond pattern at the ligand-receptor interface. Earlier studies have indicated that the difference in activities of different AlaR inhibitors are primarily due to their binding orientations and spatial arrangement towards Lys42, Tyr46, Arg140, His172, Tyr175 and Tyr364 core residues and formation of hydrogen bonding network and hydrophobic interaction^{4,6,7,9} within the catalytic pocket. In the present investigation, inhibitors binding to the MtAlaR were observed to be driven by the π - π stacking, π -cation and hydrogen bonding interactions with the conserved residues near to the PLP390. It is important to note that none of the selected inhibitors showed any interaction with the co-factor PLP390. To explain the binding mode, compounds 10, 19, 21 and 25 were selected for more detailed analysis. Figure 1d shows the docked pose of the most active compound 25 $(IC_{50} 0.03 \mu M)$ within the active site of 1XFC protein. Precisely, fifth position >C=O of thiadiazolidine-3,5-dione ring accepted a hydrogen bond from the backbone OH of Tyr175 (OH···O=C<, 2.1 Å). Another hydrogen bonding interaction was observed between third position >C=O of thiadiazolidine-3,5-dione ring and the side chain NH of Met173 (NH···O=C<, 2.0 Å). These hydrogen bonds are important for positioning and orienting the thiadiazolidine-3,5-dione ring of this inhibitor closer for π - π interactions with imidazole ring of His172 and phenyl ring of Try175. In another high active compound 19 (Figure 1b, IC₅₀ 0.05 μ M), a total of three hydrogen bonds were observed with 1XFC. The nitro oxygen atom of 2-chlorophenyl-4-nitrophenyl moiety accepted hydrogen bond from the side chain NH of Asn141 (NH····⁻O(NO), 1.8 Å). Carbonyl oxygen atoms of thiadiazolidine-3,5-dione ring exhibited hydrogen bonding interactions one each with the side chain imidazole ring NH of His172 (rNH···O=C<, 2.1 Å) and the side chain OH of Tvr46 (OH···O=C<, 2.1 Å). Our Glide XP-docking also exposed two π - π stacking interactions of this inhibitor. Phenyl ring of 2-chlorophenyl-4-nitrophenyl moiety and phenyl ring of 2,3-dihydro-1*H*-indene moiety exhibited π - π interactions, respectively with imidazole ring of His172 and phenyl ring of Tyr175. These attractive and non-covalent interactions are responsible for further stabilization of inhibitor 19 at the active site. In the lowest active inhibitor 21 (Figure 1c, IC₅₀ 28.76 μ M), only one π -cation interaction was observed between thiadiazolidine-3,5-dione ring and nitrogen atom of Lys42 side chain NH2. For this inhibitor, hydrogen bonding and π - π stacking interactions were not observed and probably this may be the reason for the lower activity of this compound. In case of another less active compound 10 (Figure 1a, IC₅₀ 13.1 μM) a single hydrogen bond was observed. Precisely, (carbamothioylsulfanyl)acetic acid moiety NH formed a hydrogen bond with the side chain imidazole ring nitrogen of His172 ($r = N \cdot \cdot \cdot NH - C(=S)S - \cdot$) (2.0 Å). This compound also showed a π - π stacking interaction of its pyridine ring with indole phenyl ring of Trp88. However, like high active inhibitors 19 and 25, no π - π stacking interactions with Tyr46, His172 and Tyr175 residues were observed for this inhibitor. It is evident from the docking results that apart from the hydrogen bonding network, π - π stacking interactions with Tyr46, His172 and Tyr175 residues are important for the stabilization within the catalytic pocket and inhibitory activity of MtAlaR inhibitors.

As shown in supplementary figure S3b, **25** fully occupied the binding pocket and oriented in a way to block the approach of substrate near to the Lys 42 and co-factor PLP390. Moreover, the positively charged (blue colour) Lys42 residue is in the region of negative (red colour) surface electrostatic potential of **25**, which favour the stabili-

zation of this inhibitor within the catalytic pocket. While the inhibitor **21**, did not occupy the whole binding pocket (Supplementary figure S3a) and oriented in a way that indene ring is exposed to the solvent pocket, disfavouring the binding of this inhibitor. Further, it can be seen from the supplementary figure S3c that inhibitors **19** and **25** phenyl rings are in close contact with the hydrophobic pocket, while the thiadiazolidine-3,5-dione rings are buried in the hydrophilic pocket. In case of inhibitor **21**, part of the 2,3-dihydro-1*H*-indene ring is buried in hydrophilic pocket while, the ethyl carboxylate group is located within the hydrophobic pocket (Supplementary figure S3c), disfavouring the binding.

3. 2. Binding Free Energy Calculation

To get a quantitative comparison of the binding strengths between diverse structure inhibitors **1-25** and 1XFC, the binding free energies (ΔG_{binds}) were computed by using the MM-GBSA approach (Li *et al.*, 2011). In the present study a moderate correlation ($R^2 = 0.573$) was observed between the computed ΔG_{binds} and IC₅₀ values of selected inhibitors **1-25**. It is evident from the energy components of the calculated binding free energies (Table 1)

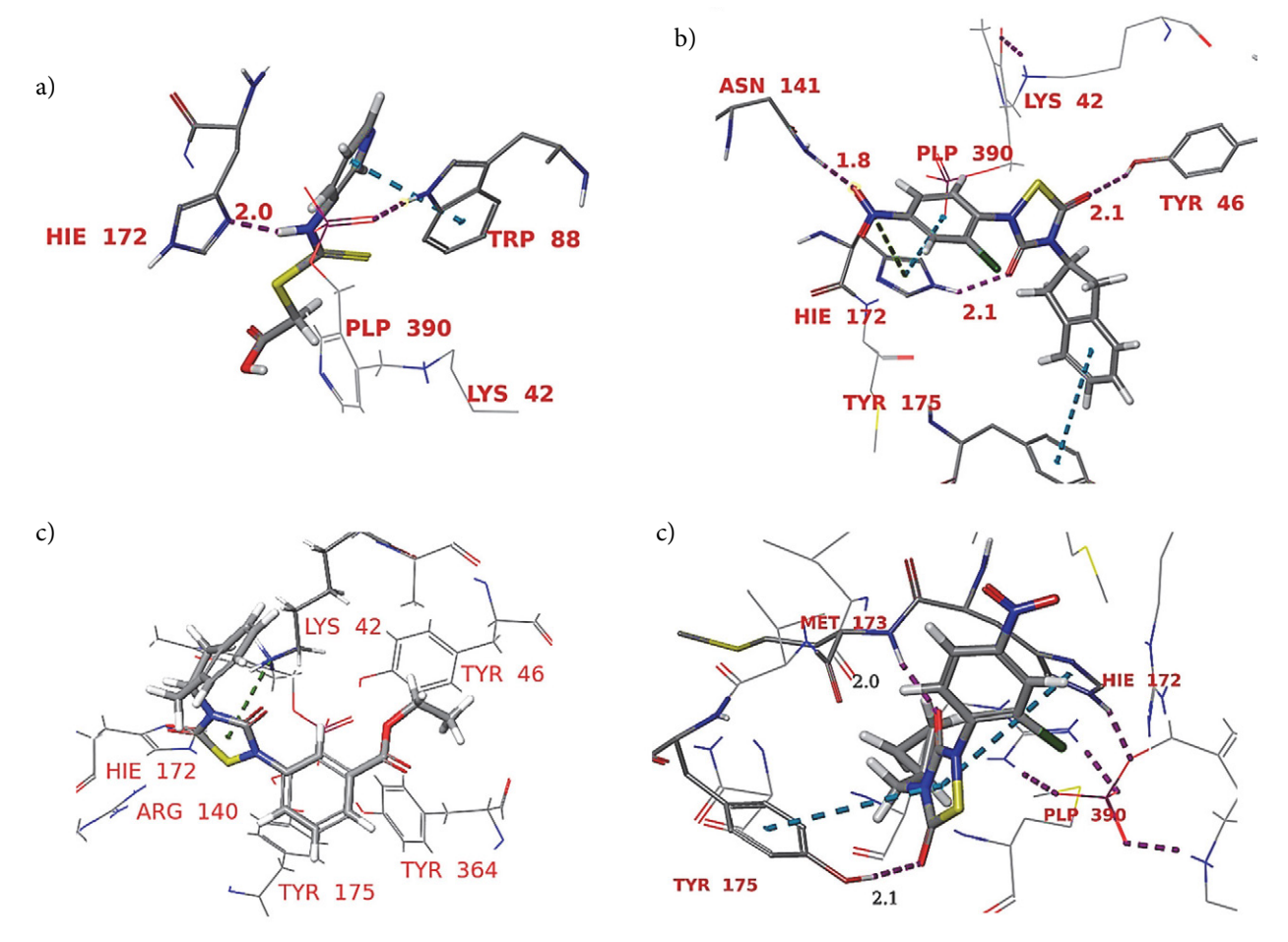


Figure 1: Binding modes of compounds (a) 10 (b) 19 (c) 21 and (d) 25 in the catalytic pocket of M. tuberculosis AlaR enzyme (PDB ID: 1XFC).

Table 1: Contribution to the free energy of binding (mm-gbsa) for ligands 1-25 with 1XFC (kcal/mol).

Compd.	IC ₅₀ (μM)	$^{a}\Delta G_{Coul}$	^b ΔG_{Cov}	$^{c}\Delta G_{H-bond}$	$^d\Delta G_{vdW} \\$	$^{e}\Delta G_{ ext{Lipo}}$	$^{\mathrm{f}}\Delta\mathrm{G}_{\mathrm{Solv}}$	$^{g}\Delta G_{bind}$
No.								
1.	5.2	-33.713	2.605	0.317	-23.690	-21.036	13.815	-60.087
2.	8.2	-29.817	-1.214	-0.428	-21.324	-22.045	28.677	-45.4426
3.	1.0	-43.348	-1.849	-5.124	-31.954	-21.937	39.614	-53.3249
4.	5.7	-48.829	-2.445	-0.657	-10.810	-14.137	29.585	-48.7813
5.	0.12	-14.652	8.125	-0.322	-27.265	-29.148	17.119	-45.1766
6.	4.48	-25.131	15.666	-1.376	-27.085	-34.652	23.502	-47.7372
7.	3.3	-3.618	-1.077	0.797	-24.274	-25.189	12.226	-41.4227
8.	6.5	21.218	-21.045	0.975	-26.127	-31.154	1.225	-56.0666
9.	9.0	77.783	-1.501	1.083	-31.825	-26.723	-23.612	-32.1513
10.	13.1	-9.601	6.504	-1.333	-20.895	-9.6544	19.690	-21.5392
11.	0.82	-9.454	-3.512	0.927	-25.370	-38.742	8.915	-61.989
12.	0.29	-54.104	24.440	-2.991	-25.605	-33.075	22.886	-57.7316
13.	2.6	-13.699	5.534	-1.351	-10.300	-18.288	-1.185	-41.3644
14.	8.2	-8.832	6.480	-1.556	-32.968	-32.636	24.397	-51.4349
15.	1.46	-40.730	6.015	-2.836	-26.248	-35.996	39.831	-59.7989
16.	0.13	3.913	-1.156	0.893	-27.383	-28.121	13.004	-42.6172
17.	4.9	20.307	1.304	-0.315	-17.582	-22.819	-30.085	-50.5578
18.	6.8	24.923	6.666	-2.189	-27.740	-18.081	-8.493	-29.8858
19.	0.05	-18.082	-4.375	-0.779	-22.054	-33.262	16.623	-63.3841
20.	6.0	8.003	-9.162	0.950	-20.613	-27.058	-1.843	-48.2484
21.	28.76	-8.562	-6.816	-1.094	-17.350	-26.901	15.372	-33.1315
22.	2.8	-1.611	-7.988	-3.683	-16.635	-10.579	6.723	-36.685
23.	0.17	0.258	-3.931	-0.221	-19.133	-26.945	-4.626	-57.9106
24.	1.6	6.098	5.407	-0.682	-29.088	-30.205	-26.703	-58.8693
25.	0.03	-23.355	3.334	-0.215	-24.938	-29.498	25.507	-63.1989

^a Coulomb energy; ^bcovalent energy (internal energy); ^chydrogen bonding; ^dvan der Waals energy; ^ehydrophobic energy (nonpolar contribution estimated by solvent accessible surface area); ^ffree energy of binding; ^gelectrostatic solvation energy.

that the major favourable contributors to ligand binding are van der Waals (ΔG_{vdW}) and nonpolar solvation (ΔG_{lipo}) terms. Whereas in all active inhibitors covalent and electrostatic solvation (ΔG_{solv}) energy terms strongly disfavour the inhibitor binding except inhibitors 9, 17, 18 and **24** which showed moderate (ΔG_{solv}) energy terms. The highly active inhibitors 19 and 25 (IC₅₀ 0.05 and 0.03 μ M respectively) showed a slightly higher van der Waals (-22.05 and -24.938 kcal/mol, respectively) and nonpolar solvation (-33.26 and -29.49 kcal/mol, respectively) contributions. Also, both inhibitors exhibited higher favourable Coulomb energy terms (-18.082 and -23.355 kcal/mol, respectively) compared to the other less active inhibitors 10 and 21 (-9.601 and -8.562 kcal/mol, respectively). It is clearly evident from result that ΔG_{vdW} and ΔG_{lipo} terms are the driving force for ligand binding and this is in well agreement with our XP-Glide docking result (Supplementary Table S2).

3. 3. Quantum Chemical Parameters

The mean electrostatic potential (ESP) of potent inhibitors **19** and **25** are +3.55 and +4.45 kcal/mol, respectively, clearly indicating that positive electrostatic potential of molecules will favour the binding of inhibitors into the

binding pocket of MtAlaR. The negative electrostatic potential of inhibitor 8, 10 and 21 (-0.03, -71.79 and -0.12 kcal/mol, respectively) may be one of the reason for low inhibitory activity (IC₅₀ 8.2, 13.1 and 28.76 μM, respectively) against 1XFC. In addition, the similarity in electrostatic potential profile of compound 19 and 25 was akin to the similarity in the inhibitory activity (IC₅₀ 0.05 and 0.03) μM, respectively) against MtAlaR enzyme. The quantum chemical calculation results show that the optimizations of ESP may lead to the potent MtAlaR inhibitor. It is evident from supplementary Table S3 that in high active compounds 19 and 25, the high negative E_{LUMO} (-1.555 and -1.630 eV, respectively) and positive nucleophilic superdelocalizibility (703.455 and 178.047, respectively) favours the inhibitors binding. Whereas in the less active compounds 10 and 21 positive E_{LUMO} (1.810 and 0.681 eV, respectively) and negative nucleophilic superdelocalizibility (-8.571 and -79.09, respectively) disfavour inhibitor binding into the catalytic pocket of 1XFC.

It appears from the LUMO shape that the molecular orbital involved in bonding with the catalytic pocket residues is located on the 2-(2-chloro-4-nitrophenyl)-1,2,4-thiadiazolidine-3,5-dione ring of compounds 19 and 25, but it is spread over the 3-aminopyridine ring in case of compound 10. The relative smaller size of LUMO lobes in com-

pound **10** explains the low inhibitory activity of this compound. A plot of the LUMO vs. HOMO energies (Supplementary figure S6) showed statistically significant correlation coefficient of $R^2 = 0.71$ with a slope and intercept of 0.67 and 5.14 eV, respectively. The slope showed consistent increase in the excitation binding energy with increasing electron affinity. These data indicates that the potent molecules should have a higher negative E_{LUMO} , positive nucleophilic superdelocalizibility and positive ESP values for the inhibitory activity. This is in well agreement with the MM-GBSA result where Coulomb energy term favours binding of compounds **19** and **25** in the catalytic pocket of 1XFC.

3. 4. Molecular Dynamics Studies

A 10 ns molecular dynamics (MD) was performed to explore the atomic details of molecular interactions. Root

mean square deviations (RMSD) from the starting structures were analysed to explore the dynamic stability of systems. The convergence of RMSD values (Figure 2a-d) at approximately 2 ns of the simulation time indicates that the systems were well equilibrated and have attained stability. The time-dependent average RMSDs of **10**, **19**, **21** and **25**/1XFC complexes backbone (0.37, 0.26, 0.74, 0.605 Å) and C- α (0.38, 0.345, 0.72, and 0.61 Å) atoms indicated less conformational changes in protein during MD simulation. It is also evident from the RMSD plots (Figure 2a-d) that the tendency of catalytic pocket residues RMSD copes well with the ligand movement. During MD simulations ligands **10**, **19**, **21** and **25** showed conformational variations up to 2 ns and then were stable for rest of the simulation period.

The protein backbone, $C-\alpha$ and heavy atoms of ligand binding residues for complexes **10**, **19**, **21** and **25**/1XFC showed root-mean-square fluctuations (RMSF)

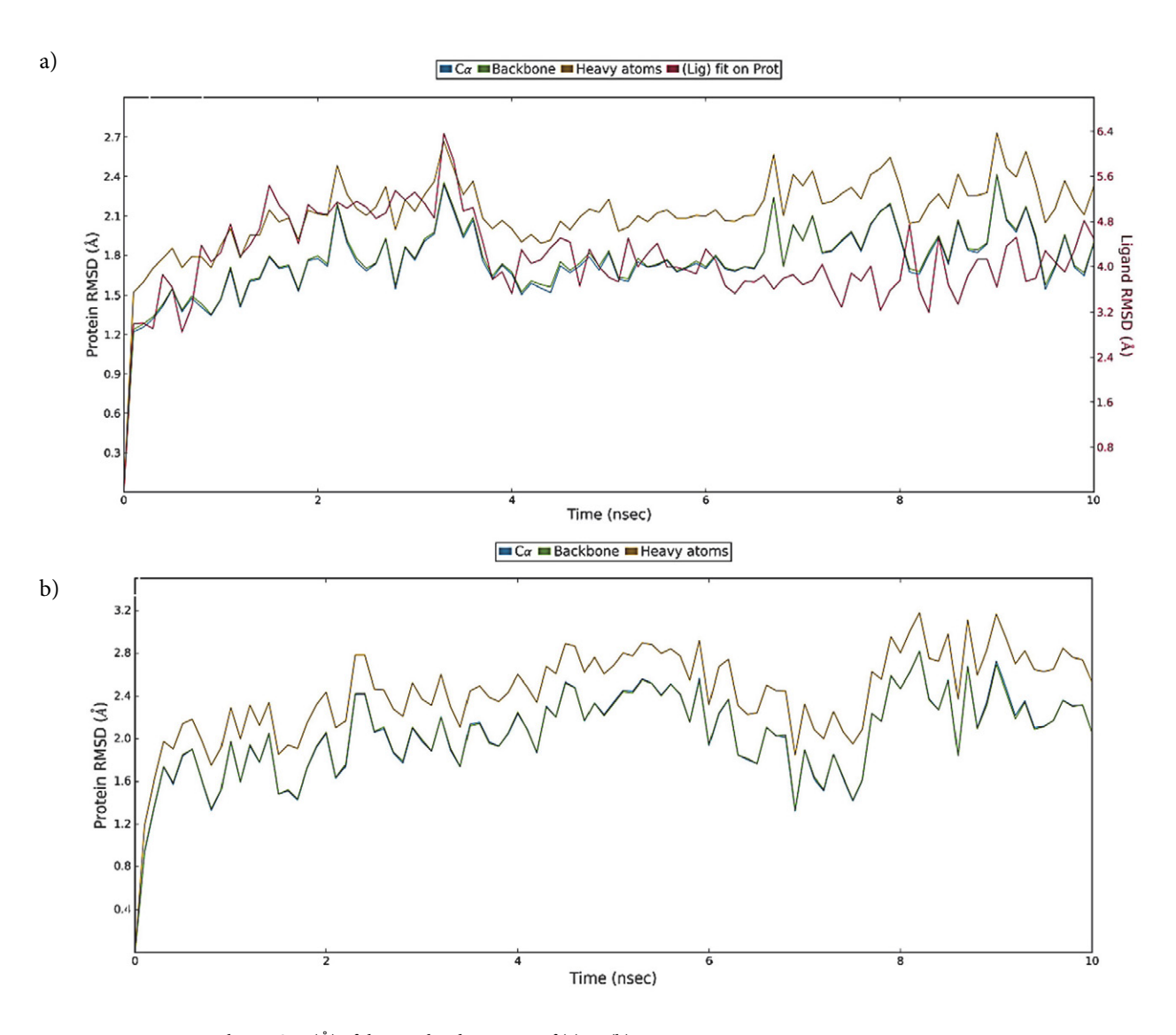


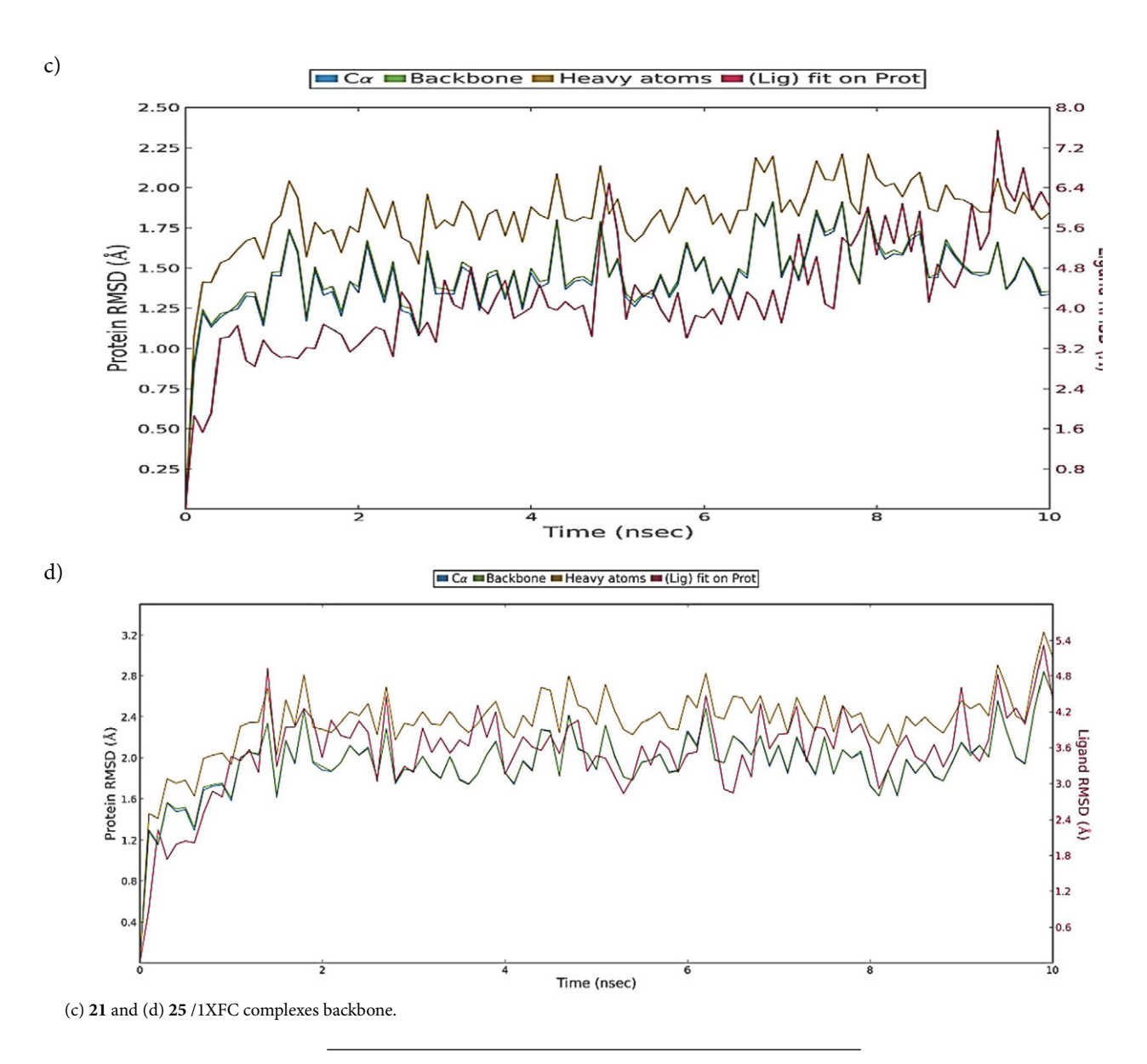
Figure 2: Represents the RMSDs (Å) of the simulated positions of (a) 10 (b) 19

values in the range 0.62–2.87, 0.5–2.10 and 0.48–3.13 Å, respectively (Figure 3a-d) which is indicative of the moderate fluctuations in these residues. The high fluctuations in RMSFs of **10**, **19**, **21** and **25**/1XFC complexes backbone (2.55–2.91, 2.87–2.96, 2.98–3.32 and 1.76–1.86 Å, respectively) and C- α (2.51–2.89, 2.61–2.88, 2.86–3.11 and 1.72–1.83 Å, respectively) atoms were observed inflexible loop between amino acid stretch Ser270 to Thr274, connecting two short β -sheets (amino acid stretches Trp275-Ile276 and Val269-Gly268). These residues are away from the catalytic pocket.

During MD simulation the low mean fluctuations of radius of gyration (rGyr) in the backbone (blue circle, 0.677 and 0.30 Å, respectively) and $C\alpha$ (red thin diamond, 0.35 and 0.31 Å, respectively) atoms for **19** and **25**/1XFC complexes (Supplementary figure S7b and S7d) further indicated low degree of flexibilities in protein complexes. However, in **10** and **21**/1XFC complexes, a little higher

mean fluctuations of rGyr in the backbone (0.677 and 1.0 Å, respectively) and $C\alpha$ atoms (1.37 and 0.81 Å, respectively) (Supplementary figure S7a and S7c) showed higher degree of flexibilities in protein complexes. These results indicate that the whole 19 and 25/1XFC systems were in more relaxed conformations compared to the 10 and 21/1XFC complexes. In comparison to the protein crystal structure average B-factor (28 Å²), a little higher average B-factor of 30.26 $Å^2$ was observed for the catalytic pocket residues during MD simulations of four complexes. During MD simulations of all four complexes, five residues Gly137, Leu138, Asn139, Arg140 and Asn141 located on the flexible loop between amino acids stretch Asp135-Gln147 showed higher B-factor in the range 48.40-74.30 Å² but lower RMSF values for the protein backbone and Cα atoms (0.68–1.46 Å and 0.67–1.31 Å, respectively).

MD simulations of **10**, **19**, **21** and **25**/1XFC complexes showed similar binding interactions as predicted in

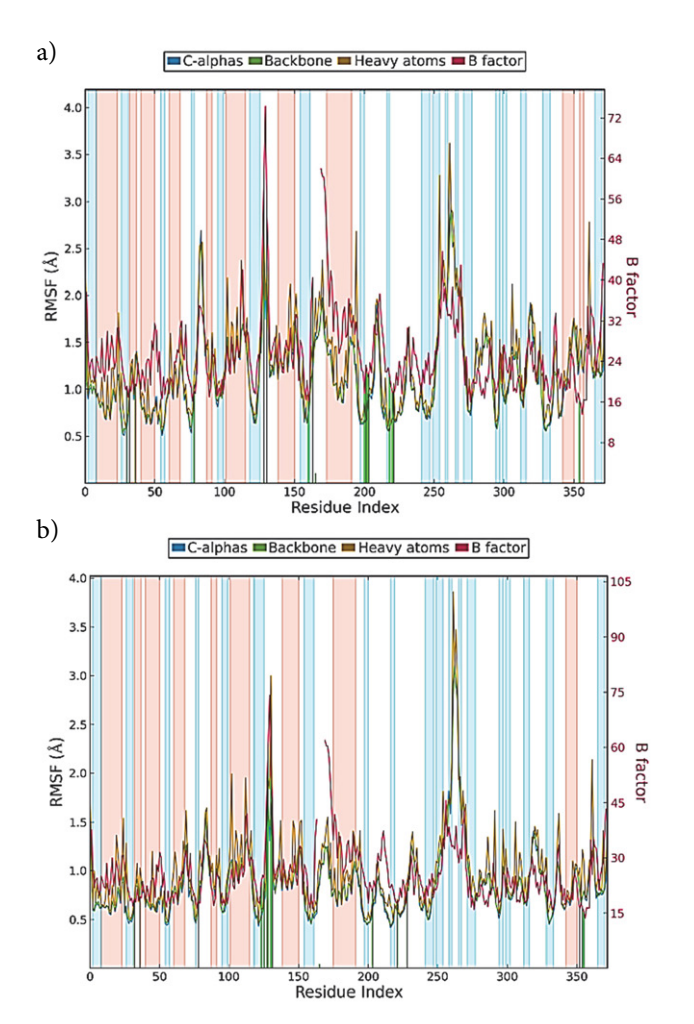


Jayaram and Azam: Computational Molecular Modeling Studies of Some ...

the extra-precision molecular docking. During MD simulation of 19/1XFC complex, all three hydrogen bonds (Asn141 NH····O(NO), His172 rNH···O=C< and Tyr46 OH···O=C<) predicted in the XP molecular docking was preserved, respectively in 7, 34 and 62% of MD trajectory (Figure 4b also Supplementary figure S8b and S9b). For this inhibitor a strong hydrogen bond interaction was observed between fifth position >C=O of thiadiazolidine-3,5-dione ring and the backbone OH of Tyr46 (>C=O···HO) (~62% of the trajectory) in a bidentate manner. Another moderate frequency hydrogen bonding interaction was observed between third position >C=O of thiadiazolidine-3,5-dione ring and the side chain NH of His172 ring (>C=O···HNr) (~34% of the trajectory). Conformational flexibility of His172 side chain ($\psi = 110^{\circ}$, Supplementary figure S10b) was observed to be less during first 8.5 ns of simulation and it is considerably less for this inhibitor compared to conformational flexibility of His172 observed for the lowest active inhibitor 10. These hydrogen bonding networks stabilized the positions of thiadiazolidine-3,5-dione and 4-nitro-2-chlorophenyl rings for π -π stackings respectively, with Tyr364 phenyl (~21% of the trajectory) and His172 imidazole (~26% of the trajectory) rings. Additional stabilization was achieved by the

low frequency π - π stacking of 2,3-dihydro-1H-indene phenyl ring with Tyr175 (~11% of the trajectory) and hydrogen bonding network between the backbone of Tyr175 and third position >C=O of thiadiazolidine-3,5-dione ring (~13% of the trajectory). These low frequency interactions are due to the conformational flexibility of Tyr175 backbone brought about by the flexible body movement of the Ser171-Asp181 stretch in loop. Our MD simulation result also exposed salt bridge interaction of nitro oxygen atom with Arg140 (~21% of the trajectory). Another salt bridge interaction was observed between oxygen atom of fifth position >C=O of thiadiazolidine-3,5-dione ring and Lys42 (~13% of the trajectory). These interactions are in good agreement with the calculated ΔG_{binds} value of this inhibitor (Table 1). These hydrogen bonds, hydrophobic and salt bridge interactions are responsible for the stabilization of this inhibitor within the catalytic pocket.

During MD simulation of the highest active inhibitor 25/1XFC complex, among the two hydrogen bonds (Tyr175 OH···O=C<, Met173 NH···O=C<) predicted in XP-docking, only one (Met173 NH···O=C<) was preserved in 37% of MD trajectory (Figure 4d also Supplementary figure S8d and S9d). A moderate frequency hydrogen bond was observed between the second position >C=O of



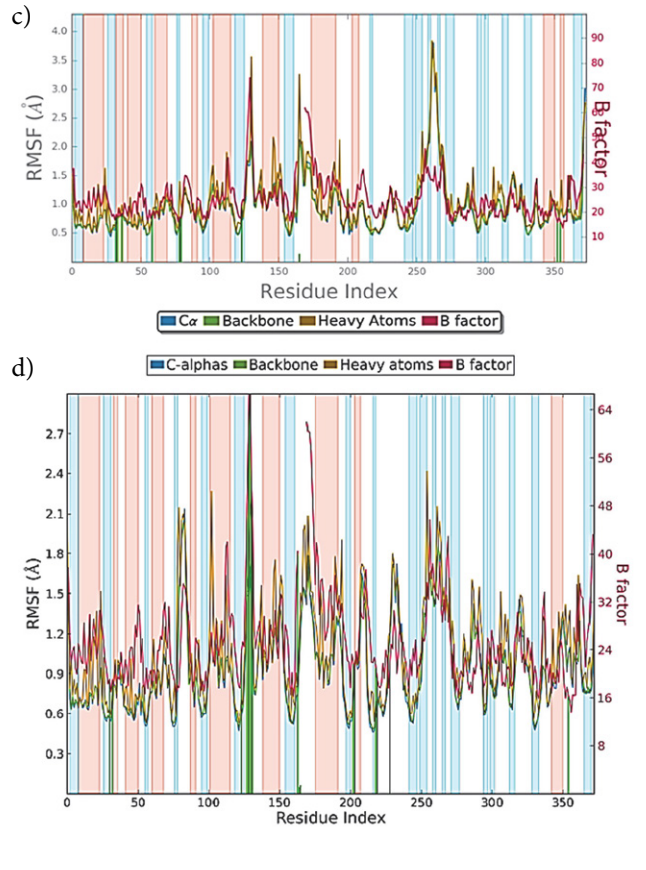


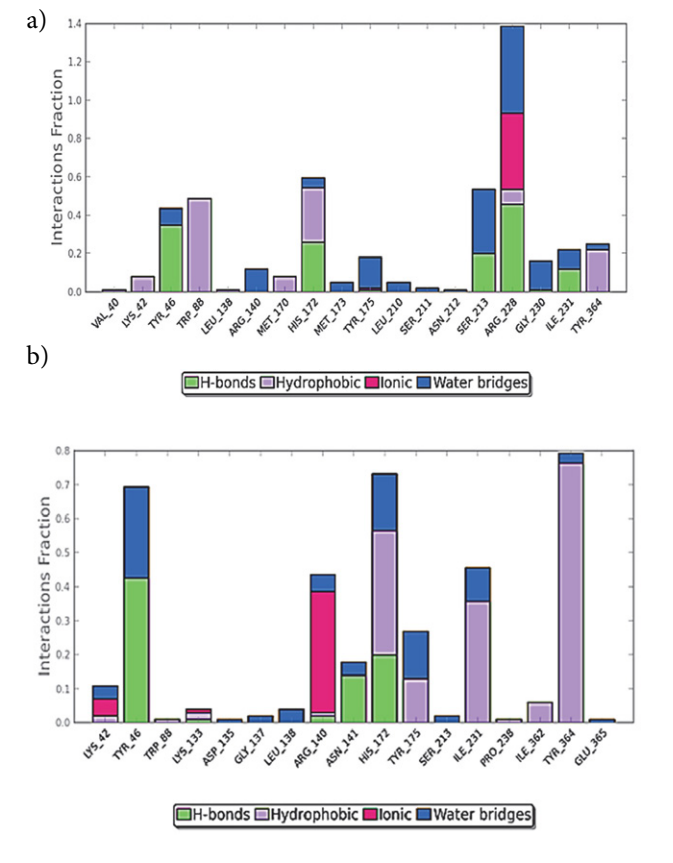
Figure 3: Represents the RMSFs (Å) of the simulated positions of (a) **10** (b) **19** (c) **21** and (d) **25**/1XFC complexes backbone atoms from those in the initial structures.

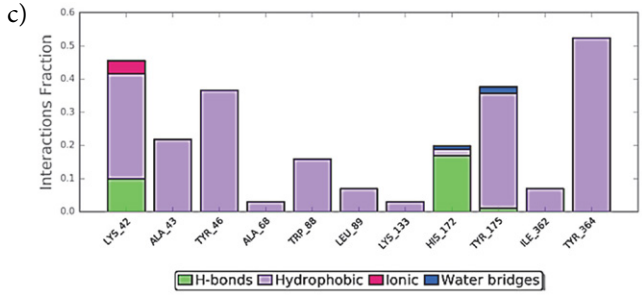
thiadiazolidine-3,5-dione ring and backbone NH (r >C=O···HN) of Met173 (~37% of the trajectory). Precisely, fifth position >C=O of thiadiazolidine-3,5-dione ring formed low frequency hydrogen bond networks with the side chain of Asn212 (>C=O···HN(H)- and >C=O···H-O-H...HN(H)) in a bidentate manner (~18% of the trajectory). Imidazole ring of His172 residue exhibited weak π - π stacking interactions, one each with thiadiazolidine-3,5-dione and phenyl rings of inhibitor 25. This weak interaction is due to the higher conformational flexibility of His172 side chain ($\psi = 340^{\circ}$, Supplementary figure S10d during first 5 ns of MD simulation and then ($\psi = 80^{\circ}$) during further last 5 ns. These hydrophobic interactions further stabilized the inhibitor 25 in the catalytic pocket of 1XFC and positioned the inhibitor near to the Lys42 and PLP390. Additionally, nitro group of 2-chloro-4-nitrophenyl moiety showed two moderate frequency water mediated hydrogen bonding networks with the side chain of Lys133 (~21% of the trajectory), back bone of Arg140 (~29% of the trajectory) and a low frequency water mediated hydrogen bonding interaction with the backbone of Leu138 (~18% of the trajectory) during MD simulation. These hydrogen bonding networks probably forms the basis for the high activity of this inhibitor compared to the low active compounds 10 and 21.

For the low active 10/1XFC complex, one hydrogen bond (His172r =N···NH-C(=S)S-), predicted in glide XP-docking simulation was preserved in 25% of MD simulation trajectory. This inhibitor exhibited a total of six

moderate to low frequency hydrogen bonds (Figure 4a, also Supplementary figure S8a and S9a). Precisely, nitrogen of pyridine ring accepted a moderate frequency hydrogen bond from the side chain of Arg228 (~45% of the trajectory) and also exhibited salt bridge interaction (~39% of the trajectory) with the same residue. These interactions stabilize the position of the pyridine ring with regard to the Trp88 phenyl and His172 imidazole rings to form low frequency π - π stacking interactions. His172 imidazole ring nitrogen atom also accepted a low frequency hydrogen bond (~25% of the trajectory) from the NH of (carbamothioylsulfanyl)acetic acid moiety (r =N···HN) of this compound. This low frequency hydrogen bond is due to the higher conformational flexibility of His172 side chain $(\psi = 350^{\circ}, \text{Supplementary figure S10a})$ during last 4 ns of simulation. This conformational flexibility is brought about by the flexible body movement of the Ser171-Asp181 stretch in loop. Another moderate frequency hydrogen bond was observed between >C=O of carboxylate and the side chain OH (>C=O···HO) of Tyr46 (~31% of the trajectory). In addition, compound 10 showed four more low frequency hydrogen bond networks with Arg140, Ser213 and Arg228 residues.

During MD simulation of **21**/1XFC complex, the π -cation interaction between thiadiazolidine-3,5-dione ring and the side chain NH₂ of Lys42 predicted in the XP molecular docking was preserved during MD simulation (~11% of MD trajectory) (Figure 4c, also Supplementary figure S8c and S9c). An additional π -cation interaction





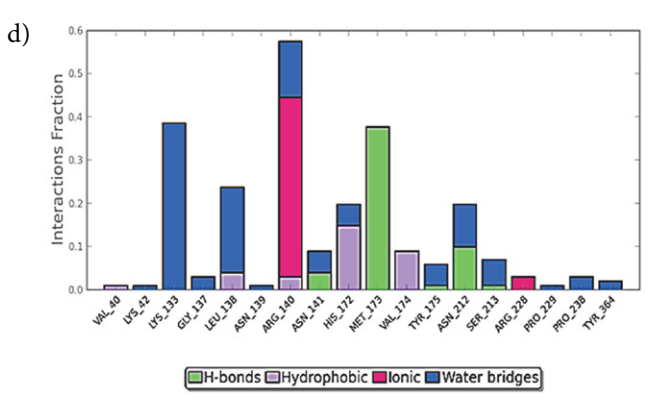


Figure 4: Plots represents interaction of compounds (a) **10** (b) **19** (c) **21** and (d) **25** with different residues of *M. tuberculosis* AlaR enzyme (PDB ID: 1XFC) throughout the simulation trajectory.

(~11% of MD trajectory) was observed between Lys42 and the phenyl ring of ethyl benzoate moiety. The side chain NH₂ of this residue also exhibited a weak hydrogen bonding interaction (~9% of MD trajectory) with position five >C=O of thiadiazolidine-3,5-dione ring. This carbonyl oxvgen atom showed another weak hydrogen bonding interaction (~16% of MD trajectory) with the side chain imidazole ring NH of His172. This low frequency hydrogen bonding interaction is due to the higher conformational flexibility of His172 side chain ($\psi = 325^{\circ}$, Supplementary figure S10c), observed during entire 10 ns MD simulation. This conformational flexibility of His172 is more compared to the conformational flexibility of His172 observed for inhibitors 19 and 25. In addition, three weak π - π stacking interactions (~5–17% of MD trajectory) were also observed for this inhibitor with Tyr46, Trp88 and Tyr175 residues. Probably these weak hydrophobic and hydrogen bonding interactions are responsible for the low activity of this compound.

The gyration radius (rGyr) measures the extendedness of a ligand. It was found to be stable after 2 ns of MD simulations of **21** and **25**/1XFC complexes and the average values were 0.215, 0.24, 0.67 and 0.11 Å, respectively (Supplementary figure S12a-d). The average RMSD of these inhibitors were 0.48, 0.465, 0.67 and 0.475 Å, respectively. As evident by the lower RMSD values, inhibitors **19** and **25** showed less conformational changes and more stability during simulation. Inhibitors **19** and **25** also exhibited lower changes in the polar surface area (PSA) (157.75–169.16 and 156.71–139.4 Ų, respectively) compared to the less active compounds **10** and **21** (MolSA: 203.5–210 and 344.6–355.58 Ų, respectively; PSA: 121.20–141.44 and 86.72–108.73 Ų, respectively) during MD simulation, fur-

ther indicating less conformational flexibility of inhibitors **19** and **25** before stabilization within the catalytic pocket.

Further, similar orientation was observed between the superposition of the conformations of **10** after MD simulation and best XP-docking pose (RMSD: 1.23 Å) (Supplementary figure S11a); conformations of **19** after MD simulation and best XP-docking pose (RMSD: 1.53 Å) (Supplementary figure S11b); conformations of **21** after MD simulation and best XP-docking pose (RMSD: 1.35 Å) (Supplementary figure S11c) and conformations of **25** after MD simulation and best dock pose (RMSD: 0.77 Å) (Supplementary figure S11d). Conformational changes of 2-chloro-4-nitrophenyl moiety arising due to the rotation about PhC-N< thiadiazolidine-3,5-dione ring bond probably resulted in slightly higher RMSDs after superposition of the conformations of **19** best XP-docking pose with the pose of MD simulation.

The designing of novel MtAlaR inhibitors targeting the blockade of bacterial AlaR enzyme is considered to be a futuristic approach as reflected by the availability of limited number of known inhibitors. The only marketed drug D-cycloserine however, faces the issues associated with the lack of target specificity and selectivity. The partial agonism offered at the glycine site of NMDA receptor and non-selective inhibition towards other PLP dependent enzymes are proven causes for the concerned drawbacks. For further evaluation, the results of the current study were compared with the AlaR inhibitory activity of the literature molecules as reported by Anthony K.G. et al. ^{24,27} The compound **19** (IC₅₀ = 0.05 μ M) and **25** (IC₅₀ = 0.03 μ M) showed potent activity against the MtAlaR. The compounds (19; $IC_{50} = 0.36 \,\mu\text{M}$) and 25; ($IC_{50} = 0.49 \,\mu\text{M}$) were also able to exhibit prominent inhibitory activity against

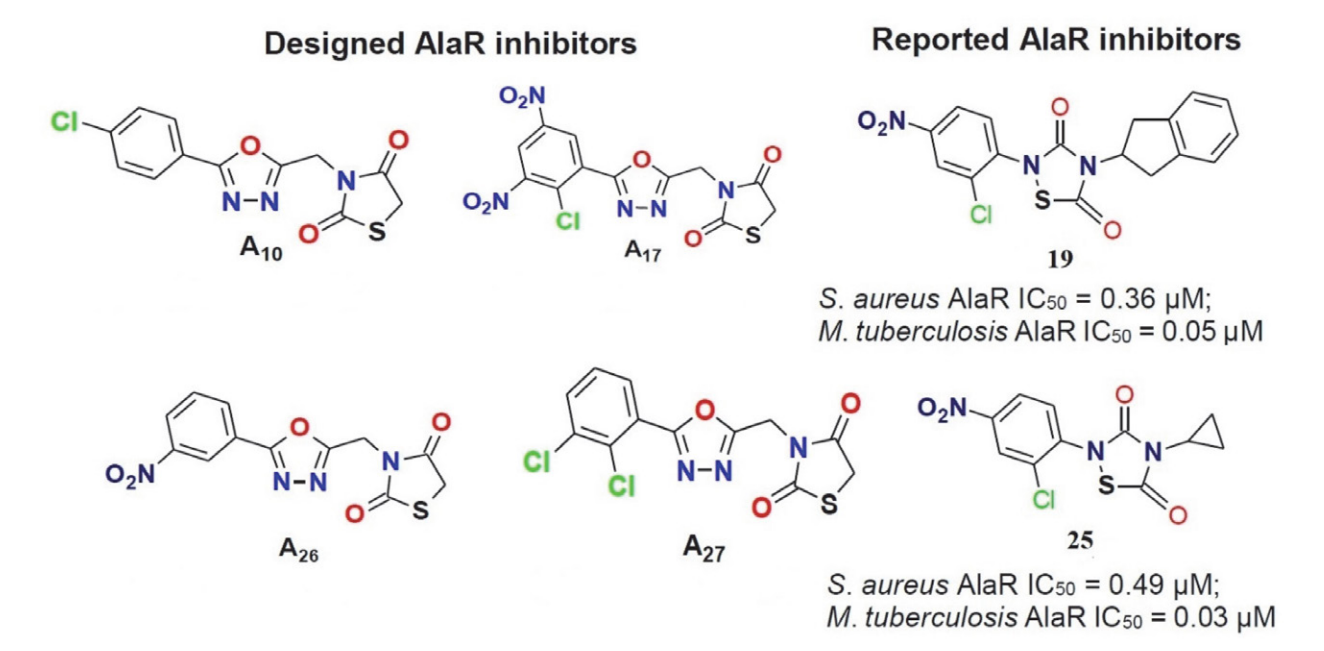


Figure 5: Structural comparison of designed AlaR inhibitors $(A_{10}, A_{17}, A_{26} \text{ and } A_{27})$ with that of reported AlaR inhibitors (19 and 25).

Staphylococcus aureus AlaR. When the structural aspects of the inhibitors 19 and 25 were compared, it was found that, three ring system scaffold, aryl ring with electron withdrawing groups like -Cl and -NO2, and thiazolidin-2,4-dione/thiadiazolidine-3,5-dione ring scaffold are essential requirements for imparting the activity (Figure 5). The reported molecule although showed high inhibitory action towards MtAlaR, but their further development as drug candidate still needs to be investigated in terms of target specified action and non-interaction with other PLP dependent enzymes. Based on the above observation, some novel AlaR inhibitors $(A_{10},\,A_{17},\,A_{26}$ and $A_{27})$ were designed which may be considered as promising lead molecules for AlaR inhibitory action. These designed molecules may assure target selectivity and enzyme inhibitory action which has to be evaluated by computational protocols and in vitro enzymatic assays.

4. Conclusion

To date, most known inhibitors of alanine racemase bind solely to the substrate binding region proximal to the PLP. In the present study, a combined computational approach was applied to gain insight into the structural basis for MtAlaR inhibitors. We obtained several possible binding poses for structurally diverse set of 25 MtAlaR inhibitors using Glide XP-docking. Docking interaction profile showed that residues Lys42, Tyr46, Arg140, His172 and Tyr175 are mainly responsible for the stabilization of inhibitors within the catalytic pocket. MM-GBSA rescoring result revealed that ΔG_{vdW} and ΔG_{lipo} terms are the driving force for ligand binding. Further, the negative values of van der Waals (ΔG-_{vdW} -22.05 and -24.93 kcal/mol, respectively) and non-polar solvation (ΔG_{Lipo} -33.26 and -29.49 kcal/mol, respectively) binding energy terms for the high active inhibitors 19 and 25, also indicated that hydrophobic interactions are primarily responsible for the stable complex formation. A computational study on inhibitors 1-25 with the B3LYP/6-31G**++ quantum chemical method was performed in an attempt to correlate stereoelectronic features with AlaR inhibitory activity. The molecular electrostatic potential of the inhibitors in specific regions of the molecules appears to play a pivotal role in the activity. Further, results showed that positive electrostatic potential, high negative E_{LUMO} and positive nucleophilic superdelocalizability favours inhibitors binding in the catalytic pocket. 10 ns MD simulations used here revealed the importance of hydrogen bonding and hydrophobic interactions of compounds with M. tuberculosis AlaR. Moreover, similar orientations were observed between the superposition of the conformations of 21 and 25 after MD simulation and respective best XP-docking poses. Based on the above finding we hereby propose the chemical structures of 4 lead molecules which may exhibit potent MtAlaR action and can be considered as a promising scaffold for further drug design and synthesis.

Acknowledgements

We would like to thank University Grants Commission (UGC), Government of India, for the financial support (No. F1-17.1/2014-15/RGNF-2014-15-SC-KER-61880).

5. References

- D. T. Hoagland, J. Liu, R. B. Lee, R. E. Lee, Adv Drug Del Rev 2016, 102, 55–72. DOI:10.1016/j.addr.2016.04.026
- N. V. Grishin, M. A. Phillips, E. J. Goldsmith, Protein Sci 1995, 4, 1291. DOI:10.1002/pro.5560040705
- A. Watanabe, T. Yoshimura, B. Mikami, H. Hayashi, H. Kagamiyama, N. Esaki, *J Biol Chem* 2002, 277, 19166–19172.
 DOI:10.1074/jbc.M201615200
- P. LeMagueres, H. Im, J. Ebalunode, U. Strych, M. J. Benedik, J. M. Briggs, H. Kohn, K. L. Krause, *Biochem.* 2005, 44, 1471– 1481. DOI:10.1021/bi0486583
- E. Davis, E. S. Hutchinson, H. O. Reading, Y. Nakatani, K. L. Krause, *Acta Cryst.* 2014, F70, 1199–1205.
 DOI:10.1107/S2053230X14017725
- P. Le Magueres, H. Im, A. Dvorak, U. Strych, M. Benedik, K. L. Krause, *Biochem.* 2003, 42, 14752–14761.
 DOI:10.1021/bi030165v
- J. P. Shaw, G. A. Petsko, D. Ringe, *Biochem.* 1997, 36, 1329– 1342. DOI:10.1021/bi961856c
- E. R. Scaletti, S. R. Luckner, K. L. Krause, *Acta Crystallogr. D. Biol. Crystallogr.* 2012, 68, 82–92.
 DOI:10.1107/S0907444911050682
- G. F. Stamper, A. A. Morollo, D. Ringe, *Biochem.* 1998, 37, 10438–10445. DOI:10.1021/bi980692s
- A. Watanabe, T. Yoshimura, B. Mikami, N. Esaki, *J. Biochem.* 1999, 126, 781–786.
 DOI:10.1093/oxfordjournals.jbchem.a022517
- S. Sun, M. D. Toney, *Biochem.* 1999, 38, 4058–4065.
 DOI:10.1021/bi982924t
- 12. D. T. Major, G. Jiali, *J. Am. Chem. Soc.* **2006**, 128, 16345–16357. **DOI:**10.1021/ja066334r
- U. Strych, M. Davlieva, J. P. Longtin, E. L. Murphy, H. Im, Benedik, K. L. Krause, *BMC Microbiol.* 2007, 7, 40–45.
 DOI:10.1186/1471-2180-7-40
- 14. T. Yoshimura, M Goto, *FEBS J.* **2008**, 275, 3527–3537. **DOI:**10.1111/j.1742-4658.2008.06516.x
- 15. F. C. Neuhaus, in: D. Gottlieb, P. Shaw (Ed.): *Antibiotics*, Springer-Verlag Berlin Heidelberg, 1967, 1, pp. 40–83.
- F. C. Neuhaus, W. P. Hammes, *Pharmacol. Ther.* 1981, 14, 265–319. DOI:10.1016/0163-7258(81)90030-9
- W. W. Yew, C. F. Wong, P. C. Wong, J. Lee, C. H. Chau, Clin. Infect. Dis. 1993, 17, 288–289. DOI:10.1093/clinids/17.2.288
- (a) M. G. Kim, U. Strych, K. Krause, M. Benedik, H. Kohn, *J. Antibiot.* 2003, 56, 160–168. DOI:10.7164/antibiotics.56.160
 (b) M. G. Kim, U. Strych, K. Krause, M. Benedik, H. Kohn, *Med. Chem. Res.* 2003, 12, 130–138.
- V. Copie, W. S. Faraci, C. T. Walsh, R. G. Griffin, *Biochem.* 1988, 27, 4966–4970.
 DOI:10.1021/bi00414a002

- M. D. Erion, C. T. Walsh, Biochem. 1987, 26, 3417–3425.
 DOI:10.1021/bi00386a025
- 21. B. Badet, D. Roise, C. T. Walsh, *Biochem.* **1984**, 23, 5188–5194. **DOI**:10.1021/bi00317a016
- F. R. Atherton, M. J. Hall, C. H. Hassall, R. W. Lambert, W. J. Lloyd, P. S. Ringrose, *Antimicrob. Agents Chemother.* 1980, 18, 897–905. DOI:10.1128/AAC.18.6.897
- F. R. Atherton, M. J. Hall, C. H. Hassall, R. W. Lambert, W. J. Lloyd, P. S. Ringrose, D. Westmacott, *Antimicrob. Agents Chemother*, 1982, 22, 571–578. DOI:10.1128/AAC.22.4.571
- 24. Y. Lee, S. Mootien, C. Shoen, M. Destefano, P. Cirillo, O. A. Asojo, K. R. Yeung, M. Ledizet, M. H. Cynamon, P. A. Aristoff, R. A. Koski, P. A. Kaplan, K. Anthony, *Biochem. Pharmacol.* 2013, 86, 222–230. DOI:10.1016/j.bcp.2013.05.004
- G. I. Mustata, T. A. Soares, J. M. Briggs, *Biopolymers*. 2003, 70, 186–200. DOI:10.1002/bip.10425
- G. I. Mustata, J. M. Briggs, J. Comput. Aided Mol. Des. 2002, 16, 935–953. DOI:10.1023/A:1023875514454
- 27. K. G. Anthony, U. Strych, K. R. Yeung, C. S. Shoen, O. Perez, K. L. Krause, M. H. Cynamon, P. A. Aristoff, A. Raymond, R. A. Koski, *PLoS One.* 2011, 6, e20374. DOI:10.1371/journal.pone.0020374
- E. Harder, W. Damm, J. Maple, C. Wu, M. Reboul, J. Y. Xiang, L. Wang, M. K. L. Dahlgren, J. L. Knight, J. W. Kaus, D. S. Cerutti, G. Krilov, W. L. Jorgensen, R. Abel, R. A. Friesner, J. Chem. Theo. Comput. 2016, 12, 281–296.
 DOI:10.1021/acs.jctc.5b00864
- G. M. Sastry, M. Adzhigirey, T. Day, R. Annabhimoju, W. Sherman, *J. Comput. Aided Mol. Des.* 2013, 27, 221–234.
 DOI:10.1007/s10822-013-9644-8
- M. P. Jacobson, D. L. Pincus, C. S. Rapp, T. J. F. Day, B. Honig,
 D. E. Shaw, R. A. Friesner, *Proteins*. 2004, 55, 351–367.
 DOI:10.1002/prot.10613

- G. N. Ramachandran, C. Ramakrishnan, V. Sasisekharan, J. Mol. Biol. 1963, 7, 95–99.
 DOI:10.1016/S0022-2836(63)80023-6
- R. A. Friesner, R, B, Murphy, M. P. Repasky, L. L. Frye, J. R. Greenwood, T. A. Halgren, P. C. Sanschagrin, D. T. Mainz, J. Med. Chem. 2006, 49, 6177–6196. DOI:10.1021/jm0512560
- 33. J. M. Wang, T. J. Hou, X. J. Xu, Curr. Comput. Aided Drug Des. **2006**, 2, 287–306. **DOI:**10.2174/157340906778226454
- 34. J. Li, R. Abel, K. Zhu, Y. Cao, S. Zhao, R. A. Friesner, *Proteins*. **2011**, 79, 2794–2812. **DOI:**10.1002/prot.23106
- A. Pullman, B. Pullman, Q. Rev. Biophys. 1981, 14, 289–380.
 DOI:10.1017/S0033583500002341
- V. Prasad, E. T. Birzin, C. T. McVaugh, R. D. van Rijn, S. P. Rohrer, G. Chicchi, D. J. Underwood, E. R. Thornton, A. B. Smith, R. Hirschmann, J. Med. Chem. 2003, 46, 1858–1869.
 DOI:10.1021/jm0205088
- 37. S. R. Gadre, P. K. Bhadane, *Reson.* 1999, 4, 14–23. **DOI:**10.1007/BF02839010
- 38. G. B. Rocha, R. O. Freire, A. M. Simas, J. J. Stewart, *J. Comput. Chem.* **2006**, 27, 1101–1111. **DOI**:10.1002/jcc.20425
- Z. Guo, U. Mohanty, J. Noehre, T. K. Sawyer, W. Sherman, G. Krilov, *Chem. Biol. Drug Des.* 2010, 75, 348–359.
 DOI:10.1111/j.1747-0285.2010.00951.x
- 40. (a) W. L. Jorgensen, J. D. Madura, *Mol. Phys.* 1985, 56, 1381–1392. DOI:10.1080/00268978500103111
 (b) C. P. Lawrence, J. L. Skinner, *Chem. Phys. Lett.* 2003, 372, 842–847. DOI:10.1016/S0009-2614(03)00526-8
- U. Essmann, L. Perera, M. L. Berkowit, T. Darden, H. Lee, L. G. Pedersen, *J. Chem. Phys.* 1995, 103, 8577–8593.
 DOI:10.1063/1.470117
- G. J. Martyna, M. L. Klein, M. Tuckerman, J. Chem. Phys. 1992, 97, 2635–2643. DOI:10.1063/1.463940
- G. J. Martyna, D. J. Tobias, M. L. Klein, J. Chem. Phys. 1994, 101, 4177–4189. DOI:10.1063/1.467468

Povzetek

Alanin racemaza je piridoksal-5′-fosfat odvisen bakterijski encim, ki zagotavlja esencialni peptidoglikanski prekurzor D-alanin, ki ga bakterija uporablja za sintezo celične stene. Ta encim je prisoten v vseh bakterijah, vključno z *Mycobacterium tuberculosis*, zaradi česar je pomembna tarča za odkrivanje novih antibakterijskih zdravil. Raziskali smo način vezave petindvajsetih znanih zaviralcev alanin racemaze bakterije *Mycobacterium tuberculosis*. Rezultati pridobljeni s študijami molekulskega prileganja so pokazali interakcije zaviralcev z aminokislinskimi ostanki Lys42, Tyr46, Arg140, His172 in Tyr175 na katalitskem veznem mestu encima alanin racemaze. Izračunane proste vezavne energije so pokazale, da predstavljajo van der Waalsove in nepolarne solvatacijske interakcije gonilno sila vezave inhibitorjev. Inhibicijski mehanizem štirih preučevanih sistemov inhibitor-alanin racemaza smo nadalje preučili s pomočjo simulacije molekulske dinamike. Kvantno kemijski parametri izračunani z B3LYP/6-31G**++ pristopom so pokazali, da morajo imeti zaviralci nizke energijske vrednosti najnižje nezasedene molekulske orbitale in visoke vrednosti elektrostatičnega potenciala za močnejše interakcije. Rezultati te teoretične študije lahko služijo kot smernica pri bodočem načrtovanju močnih zaviralcev alanin racemaze *Mycobacterium tuberculosis*.



Except when otherwise noted, articles in this journal are published under the terms and conditions of the Creative Commons Attribution 4.0 International License